Spatial epidemiological modelling of infection by Vibrio aestuarianus shows that connectivity and temperature control oyster mortality

Coralie Lupo, Bhagat Lal Dutta, Sébastien Petton, Pauline Ezanno, Delphine Tourbiez, Marie-Agnès Travers, Fabrice Pernet, Cédric Bacher

Vol. 12: 511–527, 2020
https://doi.org/10.3354/aei00379

AQUACULTURE ENVIRONMENT INTERACTIONS
Aquacult Environ Interact

Published November 19

Spatial epidemiological modelling of infection by *Vibrio aestuarianus* shows that connectivity and temperature control oyster mortality

Coralie Lupo[1,*], Bhagat Lal Dutta[1], Sébastien Petton[2], Pauline Ezanno[3], Delphine Tourbiez[1], Marie-Agnès Travers[1,4], Fabrice Pernet[2], Cédric Bacher[5]

[1]Ifremer, SG2M, F-17390 La Tremblade, France
[2]Université Brest, Ifremer, CNRS, IRD, LEMAR, 29840 Plouzané, France
[3]INRAE, Oniris, BIOEPAR, 44300 Nantes, France
[4]Université Montpellier, CNRS, Ifremer, UPVD, IHPE, 34000 Montpellier, France
[5]Ifremer, DYNECO, F-29580 Plouzané, France

ABSTRACT: *Vibrio aestuarianus* infection in oyster populations causes massive mortality, resulting in losses for oyster farmers. Such dynamics result from host–pathogen interactions and contagion through water-borne transmission. To assess the spatiotemporal spread of *V. aestuarianus* infection and associated oyster mortality at a bay scale, we built a mathematical model informed by experimental infection data at 2 temperatures and spatially dependent marine connectivity of oyster farms. We applied the model to a real system and tested the importance of each factor using a number of modelling scenarios. Results suggest that introducing *V. aestuarianus* in a fully susceptible adult oyster population in the bay would lead to the mortality of all farmed oysters over 6 to 12 mo, depending on the location in which infection was initiated. The effect of temperature was captured by the basic reproduction number (R_0), which was >1 at high seawater temperatures, as opposed to values <1 at low temperatures. At the ecosystem scale, simulations showed the existence of long-distance dispersal of free-living bacteria. The western part of the bay could be reached by bacteria originating from the eastern side, though the spread time was greatly increased. Further developments of the model, including the consideration of the anthropogenic movements of oysters and oyster-specific sensitivity factors, would allow the development of accurate maps of epidemiological risks and help define aquaculture zoning.

KEY WORDS: Basic reproduction number · *Crassostrea gigas* · Hydrodynamics · Oyster disease · Sensitivity analysis · *Vibrio aestuarianus*

1. INTRODUCTION

The Pacific oyster *Crassostrea gigas* is of primary importance for shellfish farming as it accounts for approximately three-quarters of all production in France (~486 million Euros) (FranceAgriMer 2019). Since 2008, the oyster industry has been seriously challenged by mass mortality associated with different pathogens, such as the ostreid herpesvirus OsHV-1 in spat (Segarra et al. 2010) and the bacterium *Vibrio aestuarianus* in adults in France (Garcia et al. 2014, Azéma et al. 2017), Ireland, Scotland, and Spain (EFSA Panel on Animal Health and Welfare 2015, Lasa et al. 2019). These mortality events have severe economic impacts for the oyster industry. Most *V. aestuarianus*-related mortality among adult oysters occurs in summer, and cumulative mortality can reach approximately 30% after 2–3 yr of farming (Garcia et al. 2014). During the last decade, research has mostly focused on *V. aestuari-*

*Corresponding author: clupo@ifremer.fr

Publisher: Inter-Research · www.int-res.com

anus infection burden (Parizadeh et al. 2018) and related mortality occurrence, or on the properties of the bacterium (Garnier et al. 2008, De Decker et al. 2013, Goudenège et al. 2015), but less attention has been paid to its transmission and on the implementation of efficient control measures.

Investigating the efficiency of possible disease mitigation strategies in a field setting requires considerable time and is resource-intensive and ethically undesirable. Computer-based simulation modelling is a widely acknowledged alternative approach to evaluating disease management strategies *ex ante*. It enables prioritising control strategies against pathogen spread in animal populations under different scenarios. To date, although such a modelling approach is popular in human, animal, and plant disease management (Thompson & Brooks-Pollock 2019), only a few models of marine diseases have been developed to inform evidence-based policy-making (Murray 2008, Powell & Hofmann 2015). For example, the effectiveness of several mitigation strategies against the parasite *Ciona intestinalis* in mussel populations in Prince Edward Island was compared using a mathematical modelling approach (Patanasatienkul et al. 2019). Before implementing these simulations, one must first identify the key processes involved in the disease spread and evaluate their relative importance in disease transmission and progression within hosts (Murray 2008). For example, the modelling of transmission dynamics of *Perkinsus marinus*, a well-known parasite of the eastern oyster *Crassostrea virginica*, resulted in the discovery that high oyster density could limit disease invasion through foraging interference and depletion of pathogens in the water column (Bidegain et al. 2017). Although models are imperfect representations of natural systems, they are valuable ways to integrate current knowledge and data to understand the key dynamic processes involved in ecosystem functioning. Coupled models that link biology and physical modelling are increasingly being used to simulate the dispersion and life cycle of pathogens (Salama & Rabe 2013). Coupling dispersion with epidemiological models is needed to understand feedbacks and controls of marine diseases, to forecast marine disease dynamics, and to inform effective mitigation strategies, but this remains a challenge (Ben-Horin et al. 2020).

A modelling strategy must also include some qualitative or quantitative assessment of model outputs. In human infectious disease modelling, a minority of studies have addressed the assessment of model accuracy and quality, since empirical data are scarce or highly uncertain, or the time of intervention relatively fast (Walters et al. 2018). In general, authors perform a pragmatic form of validation. In marine molluscan disease modelling, data from longitudinal studies are rarely available. Therefore, previous models were evaluated against disease prevalence monthly or yearly data collected in the field for abalone (Brandt & McManus 2009, Sokolow et al. 2009, Zvuloni et al. 2015), or cumulative mortality data from previous epizootics for eastern oysters (Bidegain et al. 2017).

In the French national context of massive oyster mortality associated with pathogen detection, an interdisciplinary project was established to observe, analyse, and assist with managing the effects of global change on oyster-farming ecosystems considering animal health and physiology as well as environment and economics (the GIGASSAT project). From 2012 to 2016, this project combined observation, experimentation, and modelling to help predict and manage oyster ecosystems. Several French marine ecosystems, in which mass mortalities of both juvenile and adult oysters were regularly reported, were monitored using sentinel oysters. Mortality was recorded and animal samples were collected for laboratory DNA detection of OsHV-1 and the bacterium *V. aestuarianus*. In particular, a longitudinal field study identified environmental risk factors of mortality in adult sentinel oysters (Gangnery et al. 2019) in an estuarine ecosystem located in the Baie des Veys, Normandy, where adult oyster mortalities due to *V. aestuarianus* are regularly reported (Garcia et al. 2014). In parallel, the transmission of *V. aestuarianus* was modelled to identify and estimate the key parameters of the infection in a small and closed oyster population under controlled laboratory conditions (Travers et al. 2017, Lupo et al. 2019). The experimental local-scale model enabled the mimicking of the oyster intra-population transmission of *V. aestuarianus* in a tank with homogeneous environmental conditions for 2 wk (Lupo et al. 2019).

We present here the upscaling of this knowledge and these processes into a disease process-based model at larger spatial and temporal scales, with the final goal of supporting decision-making. Our model accounts for larger spatial and temporal scales, heterogeneity in oyster space occupation and density, varying exposure to environmental conditions, and marine connectivity. Field data on *V. aestuarianus* infection of oysters are usually too scarce for both model parameterisation and validation. The current French surveillance system is mainly based on farmer notifications of mollusc mortality, and laboratory investigation following these notifications is not

systematic (Dufour & Hendrikx 2009). The longitudinal field study conducted in Baie des Veys (Gangnery et al. 2019) was not designed for model validation, but allowed the comparison of predicted versus observed oyster mortality patterns and related putative risk factors. Therefore, we developed our model by utilising previous studies developed as part of the GIGASSAT project regarding adult oyster mortality (Gangnery et al. 2019, Lupo et al. 2019). Our objective was to simulate the spatio-temporal dynamics of Pacific oyster mortality due to *V. aestuarianus* infection using a spatialised epidemiological model to rank the processes involved in the related disease spread in oyster populations at a bay scale. We used the model to test the hypothesis that high temperature triggers infection and mortality and we ran a large number of scenarios to assess whether some areas of our modelled system could be safe for oyster production.

2. MATERIALS AND METHODS

2.1. Study area

The Baie des Veys is located on the French coast in the western part of the English Channel and consists of 2 main farming zones: Grandcamp in the east and Utah Beach in the west (Fig. 1). This area supports important oyster farming activity conducted throughout the year by 69 different oyster farms. The Baie des Veys is one of the 9 shellfish production areas in Normandy, which is the second-largest oyster farming region in France with an annual production of ca. 9000 tons (Agreste 2015).

The Baie des Veys covers 37 km^2 and has a semi-diurnal macrotidal regime with maximum amplitudes ranging from 2.5 to 7 m during neap and spring tides, respectively (Gangnery et al. 2019). The mean daily seawater temperature varies from 7.6°C (95% CI = 7.4, 7.8) from January to March to approximately 18.7°C (95% CI = 18.6, 18.9) in August (REPHY 2017).

2.2. Model overview

The model accounts for interactions at multiple scales, including the spread of pathogens between oyster populations in an open marine system. We combined epidemiological equations of pathogen dispersion within a system under realistic forcing conditions. Starting with disease dynamics, the introduced infected oyster populations shed bacteria, which accumulate in the water and decay with time. The pathogens diffuse at the local scale and infect the neighbouring (local) oyster population. A connectivity matrix accounts for the spread of pathogens due to water movements and exposure of distant oyster populations. Therefore, the local pathogen population (i.e. bacteria concentration) depends on both the local oyster population infection dynamics and the transportation of pathogens from other oyster populations through the tidal currents. Our model includes the influence of fluctuating environmental factors, notably the seawater temperature, on the bacteria transmission. Being sessile animals, infected oysters move neither within a farm nor between farming sites on their own. Due to a lack of available data, we did not consider the movements due to farm management.

Therefore, the model involves the following 4 coupled components: (i) disease dynamics at the local population scale, (ii) temperature dependence of epi-

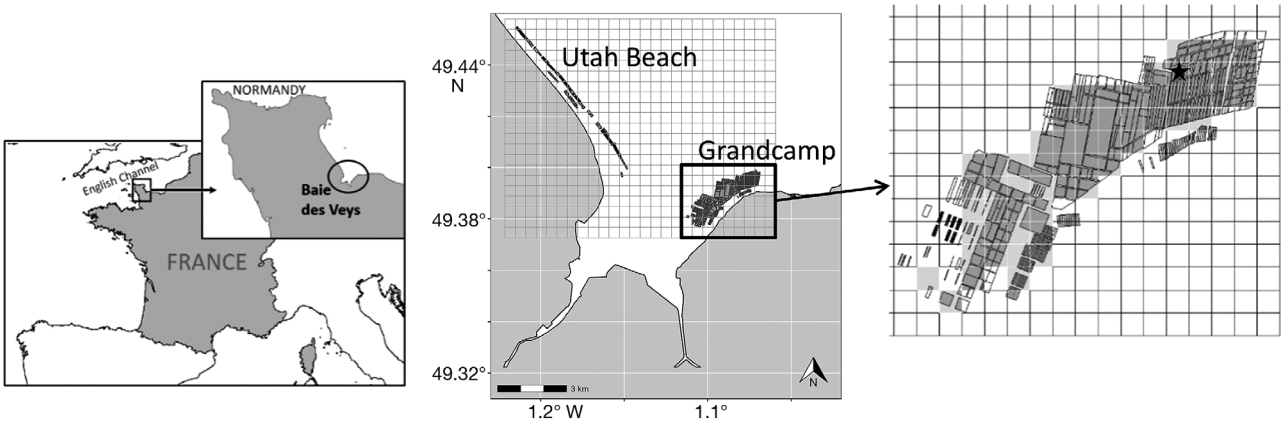

Fig. 1. Location of the study area, Baie des Veys, Normandy, France. The oyster farming zone is indicated by shading and the computation grid. The star indicates the location of patch 78

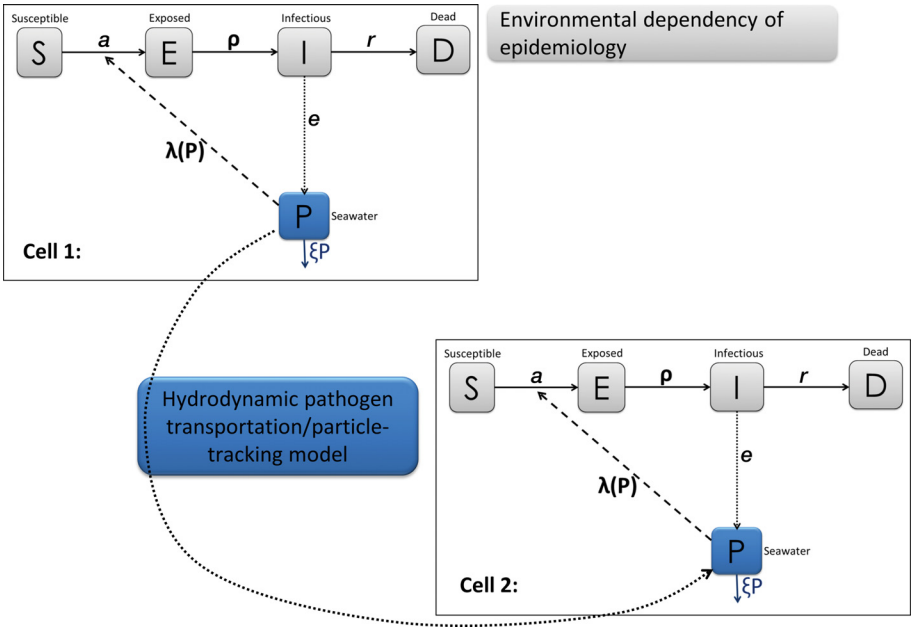

Fig. 2. Flow diagram showing the modelling framework components of *Vibrio aestuarianus* spread among oysters and in their environment. Solid arrows indicate the transitions of the oysters between the various health states. Dashed arrows represent the dynamics of the pathogen population. See Table 1 for population states and parameter abbreviations and descriptions

demiological parameters, (iii) local spread of pathogens, and (iv) tidal hydrodynamics. The modelling framework components are described in Fig. 2. The workflow of the model setup and outputs is shown in Fig. 3.

2.3. Model components and parameterisation

We used a combination of field data, experimental data, literature, and assumptions to develop a portfolio of relevant model parameters.

2.3.1. Oyster populations

In France, land for oyster production is owned by the French State and leased to farmers. This leasing ground system is regulated and georeferenced by the authorities using the maritime register. In Normandy, oysters are usually farmed in plastic mesh bags and set on trestles in the intertidal zone (Buestel et al. 2009). Oyster density is regulated by law with an authorised maximum density of 6000 bags ha^{-1} (Préfecture du Calvados 2007, Préfecture de la Manche 2013), with one bag containing on average 200 adult oysters (Girard et al. 2010). There is no natural oyster recruitment in the Baie des Veys, where the oyster populations consist only of farmed animals. We used a regular grid with a fine resolution of the study area (200 m). Based on the overlap of the maritime register as listed by the authorities and the grid cells, we defined 85 cells with oysters, named 'patches' (Fig. 1), which allowed the computing of the oyster density in each patch, which was assumed to be uniform within a patch. We hypothesised that the population was only composed of adult oysters.

2.3.2. Disease dynamics

We represented the *Vibrio aestuarianus* infection dynamics among a small-scale oyster population. Waterborne transmission of infection occurred through contact between susceptible oysters and contaminated seawater. The bacteria were shed by the infected oyster populations, accumulated in the water, and decayed over time.

We used a previously validated compartmental epidemiological model to account for the local infection dynamics at the small and homogeneous oyster population level (Lupo et al. 2019), i.e. within a patch. The model had 4 epidemiological compartments representing the susceptible (S), exposed (E), infectious (I), and dead (D) oysters, and a compartment for the free-living bacteria (P) in the surrounding water body (Fig. 2). After infection initiation, we assumed that the only outcome for an oyster was death (Azéma et al. 2015, Travers et al. 2017).

The parameters of the epidemiological model are described in Table 1. We did not account for the contribution of the dead oysters (resulting from the infection) to the water compartment, assuming the fast natural cleaning of dead oysters in the open sea.

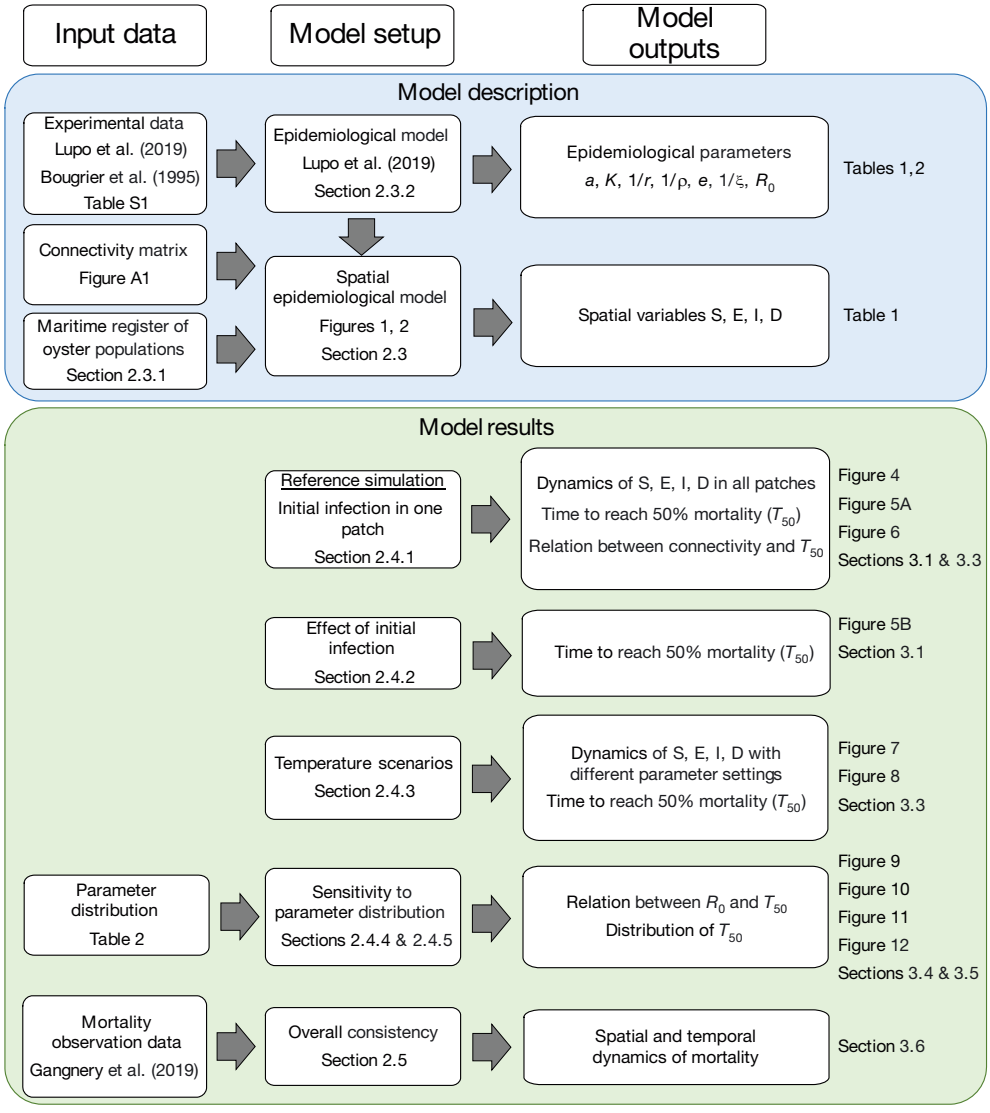

Fig. 3. Model workflow: input data, model setup, and outputs with corresponding sections, values, and results in the main text

The temporal dynamics of *V. aestuarianus* in both the oyster population and seawater were described by a system of ordinary differential equations (Table 1) in a deterministic framework, as large populations were considered. The probability of developing a *V. aestuarianus* infection $\lambda(P)$ depended on the concentration of the pathogen in the water. This dependence was represented by a logistic dose–response function (Table 1). The decay rate of *V. aestuarianus* in the seawater, ξ, included the natural mortality, sedimentation, and other stages of the bacterium that prevented its transmission to susceptible oysters.

The model was solved using a time step of 12 h, but we assumed that waterborne transmission could only occur for 6 h, corresponding to the submersion time of the patches during the semidiurnal tide cycle. We also assumed a closed homogeneous population of adult oysters.

2.3.3. Temperature effect

Dedicated experimental trials were designed to measure the epidemiological parameter values at different seawater temperatures, as previously described by Lupo et al. (2019) (Text S1 in the Supplement at www.int-res.com/articles/suppl/q012p511_supp.pdf). Seawater temperature values were roughly selected based on the temperature monitoring of the Baie des Veys coastal waters (REPHY 2017).

The model parameters were calibrated by integrating knowledge from the small-scale experimental individual transmission trials at low temperatures (i.e. merged 10°C and 15°C due to a low number of observations; Text S1) and high temperatures (i.e. 20°C) (Lupo et al. 2019).

To represent each epidemiological parameter in the model, the observed mode in the experimental

Table 1. Variables and parameters

Notation	Definition	Unit	Formulation
Population state for one patch at time *t* (d)			
S	Number of susceptible oysters	No. of ind.	$\frac{dS}{dt} = -a \cdot \lambda(P) \cdot S$
E	Number of exposed oysters, i.e. infected but not infectious oysters	No. of ind.	$\frac{dE}{dt} = -a \cdot \lambda(P) \cdot S - \rho \cdot E$
I	Number of infectious oysters that will die from the infection	No. of ind.	$\frac{dI}{dt} = \rho \cdot E - r \cdot I$
P	Concentration of bacteria in the surrounding seawater	Bacteria ml^{-1}	$\frac{dP}{dt} = e \cdot I - \xi \cdot P$
D	Number of dead oysters due to the infection	No. of ind.	$\frac{dD}{dt} = r \cdot I$
Epidemiological parameter			
a	Rate of exposure to contaminated seawater	d^{-1}	
$\lambda(P)$	Probability of an oyster being infected by contaminated water		$\lambda(P) = \frac{P}{K+P}$
K	Half-infective dose, i.e. concentration of bacteria in seawater that yields a 50% chance of infecting healthy oysters	Bacteria ml^{-1} d^{-1}	
$1/\rho$	Duration of latency period of infection	d	
$1/r$	Duration of infectious period	d	
e	Bacteria shedding rate of the infectious oysters	Bacteria ml^{-1} d^{-1} $oyster^{-1}$	
$1/\xi$	Free-living-bacteria lifetime in seawater	d	
Local contagion parameter			
R_0	Basic reproduction number of the disease	No. of ind.	$\sqrt{\frac{a.e.S_0}{r.K.\xi}}$

trials was selected as the most probable value at a low temperature class (Table 2).

The rate of exposure to the contaminated seawater at a low temperature was based on the filtration rate (clearance rate) of *Crassostrea gigas* previously estimated at 10°C (Bougrier et al. 1995).

2.3.4. Local contagion

This spatial process within the patch was modelled in an implicit way. The local spread of *V. aestuarianus* was based on the basic reproduction number, R_0, defined as the average number of secondary infections caused by one infected animal introduced to a susceptible population (Anderson & May 1991). R_0 carries information regarding the magnitude of the transmission, and its formula was formalised for *V. aestuarianus* infection among oysters (Table 1, Text S2). Its value depended on the epidemiological parameter values at the 2 temperature classes (Table 2).

Assuming that the swimming behaviour of *Vibrio* bacteria was negligible (Shigematsu et al. 1995), and that *V. aestuarianus* was not adsorbed to particles or organisms (Parizadeh et al. 2018), free-living bacteria were represented as passive particles. The concentration of bacteria within a patch was assumed to be homogeneous for a given time step.

2.3.5. Hydrodynamic transport of pathogens

Dispersal of pathogens was modelled using the transport model MARS3D, already implemented in Baie de Veys (Gangnery et al. 2019), and the regular grid of the study area (200 m) was used to define the patches.

To simulate the dispersion of pathogens, we hypothesised that the shedding moment occurred during the last hour before a high tide, when the sea reached every leasing ground. We used the same 12 hourly outputs of Eulerian transport simulations as Gangnery et al. (2019) and constructed a connectivity matrix between patches for the year 2014 in order to obtain the probability of a pathogen particle, i.e. a free-living *V. aestuarianus* bacterium, shed from one particular patch reaching another identified receiving patch (see Appendix). This enabled the calculation of the number of pathogens in each patch resulting from hydrodynamic pathogen exchange.

These calculations took into account the most probable value of the free-living bacterium's lifetime in seawater ($1/\xi$) (Table 1). Therefore, the infection dynamics occurred at time step t due to the pathogens remaining in the water compartment, i.e. accounting for daily pathogen decay, incoming pathogens, and the pathogens shed locally during time step t.

Table 2. Epidemiological parameters for simulation experiments at low and high seawater temperatures and relative difference of epidemiological parameter values used to replace the ones in the REF scenario in the different sensitivity analyses. Q1: first quartile; Q3: third quartile

Epidemiological parameter	Unit	High temperature				Low temperature				Relative parameter difference with the most probable value at high temp.		Relative parameter difference by replacing the most probable value at high temp. by the one at low temp.
		Value	Q1	Q3	Source	Value	Q1	Q3	Source	Q1 (%)	Q3 (%)	Inverse high/low (%)
Rate of exposure to contaminated water (*a*)	d^{-1}	0.75	0.61	0.91	Lupo et al. (2019)	0.59	–	–	Bougrier et al. (1995)	19	21	21
Half-infective dose (*K*)	Bacteria ml^{-1} d^{-1}	84 348	54 364	120 229	Lupo et al. (2019)	2 240 387	142 364	35 256 403	Present study	36	43	2556
Latency period (1/ρ)	d	4.5	3.25	5.00	Lupo et al. (2019)	10	9	11	Present study	28	11	122
Infectious period (1/*r*)	d	1	1.00	2.00	Lupo et al. (2019)	2	2	6.75	Present study	0	100	100
Bacteria shedding rate (*e*)	Bacteria ml^{-1} d^{-1} oyster^{-1}	72 684	12 250	167 500	Lupo et al. (2019)	193 354	11 500	277 000	Present study	83	130	166
Free-living bacteria lifetime in seawater (1/ξ)	d	1.88	1.00	3.00	Lupo et al. (2019)	4	3	4	Present study	47	60	113
R_0 (for 1 oyster S)	Number of ind.	1.10	–	–	Present study	0.64	–	–	Present study	–	–	–

2.4. Model setup

Due to a lack of information regarding the origin of the infection and a lack of data regarding observed mortality in cultivated oyster farms, this model was primarily designed to investigate the role of the simulated processes in the spatial and temporal dynamics of the infection. We established a series of scenarios mimicking the introduction of infected oysters in one location under realistic hydrodynamic conditions and assumptions involving temperature variations. The comparison of model outputs enabled the exploration of the effects of temperature, hydrodynamic connectivity, and local contagion on oyster infection and mortality caused by *V. aestuarianus*.

2.4.1. Reference simulation

The reference scenario (REF) was a standard 1 yr simulation from January to December 2014, corresponding to the longitudinal survey (Gangnery et al. 2019), with the following setup. (1) A prevalence of 50% of I oysters was introduced in patch 78 (east zone, Grandcamp) on 1 January. This is one of the patches pertaining to the Baie des Veys area, which is the bay most of the aquaculture takes place. (2) Oyster density was fixed at its maximum allowed by regulation, i.e. 6000 bags per hectare. (3) Low and high temperature cycle: the parameter values of the epidemiological model switched between low and high levels depending on the month (Table 2). In all temperature scenarios, the parameter values were spatially homogeneous but changed over time. January to June (Day 0 to 180) were assigned to low temperature (see Section 2.3.3), July to October (Day 180 to 333) to high temperature, and November and December (Day 334 to 365) again to low temperature.

2.4.2. Sensitivity to initial conditions

Similar simulations were carried out with different initial conditions. For each patch, a simulation was run where the oysters were initially infected, resulting in a set of 85 simulations. The REF simulations were used as a baseline for scenario comparisons, which were only qualitative and not quantitative.

We computed the fraction of the total oyster population in S, E, I, and D states by summing the values in all patches. The dynamics of these epidemiological states summarised the infection dynamics at the system scale. We also summarised model outputs by

computing the time to obtain 50% mortality (T_{50}) in each patch and in the whole oyster population of the bay. This metric allowed the comparison of mortality dynamics between scenarios. We repeated these simulations and calculations with each individual patch initialised with infected oysters and mapped the results. We also plotted the metric versus R_0 and connectivity.

2.4.3. Temperature scenarios

Using the same setup, we defined a set of temperature scenarios as follows: low seawater temperature (LOW), the temperature was maintained at a low value throughout the year and was spatially homogeneous throughout the study area; and high seawater temperature (HIGH), the temperature was maintained at a high value throughout the year and was considered to be spatially homogeneous throughout the study area.

2.4.4. Uncertainty analysis

To explore the effects of uncertainty regarding epidemiological parameter values, 100 simulations were run for one initial condition (patch 78) using random values of parameters drawn from their observed experimental distributions. Then, T_{50} was computed for the whole oyster population for each simulation and R_0.

2.4.5. Sensitivity to epidemiological parameters

Several simulations were run with different parameter values to assess the sensitivity of the model outputs and analyse the role of relevant epidemiological parameters (Table 2). Mean T_{50} was used as an indicator of the response of the modelled system to parameter changes. Results were likely to depend on the initial infected patch, but our simulations were deliberately restricted to the same initial condition (patch 78) to ease comparisons.

Because simulations showed that temperature was a key factor, a sensitivity analysis was first carried out to analyse the replacement of the most probable values of the epidemiological parameters by their most probable value at low temperature one at a time in the REF scenario.

In a second series of tests, the most probable values of the epidemiological parameters were replaced by the first (Q1) or third (Q3) quartile value of observed experimental distributions one at a time at high temperature in the REF scenario to assess the variability of model outputs depending on the range of input parameters.

2.5. Overall model consistency

Predicted versus observed oyster mortality patterns were qualitatively compared and the related putative risk factors were explored during the longitudinal field study in Baie des Veys, although the causative pathogen was uncertain (Gangnery et al. 2019).

Gangnery et al. (2019) monitored oyster mortality in Baie des Veys from April to October 2014 to determine the timing and spatial dynamics of sentinel oyster mortality and identify the environmental risk factors. They concluded that the mortality of adult sentinel oysters was likely caused by pathogenic bacteria. They found that adult sentinel mortalities were the lowest in Utah Beach and that mortality in some farmed areas could reach 60% or more. They distinguished 2 mortality periods with different risk factors. The first period extended from May to mid-July, and sentinel mortality was associated with connectivity to estuaries, temperature, and chlorophyll concentrations. In contrast, the second period extended from mid-July to October, and risk factors were connected to Grandcamp (in the eastern part of the bay) and salinity. However, the link to *V. aestuarianus* could not be demonstrated but was suspected. They suggested that the connectivity to the Grandcamp farmed area reflected the presence of a high-density oyster reservoir. They also highlighted that both salinity and temperature likely affect the occurrence and persistence of bacteria.

3. RESULTS

3.1. Speed of pathogen spreading and mortality outburst

The results of the REF scenario illustrate the dynamics and timing of the infection by *Vibrio aestuarianus*. Half of patch 78 was initially infected, and simulation shows a rapid decrease in S oysters, the numbers of which reached 0 after only 10 d. The number of E and I oysters also varied rapidly, and mortality dramatically increased during the first 20 d (Fig. 4). In patch 78, all of the oysters eventually died and more than 90% died within the first 50 d of the simulation. The

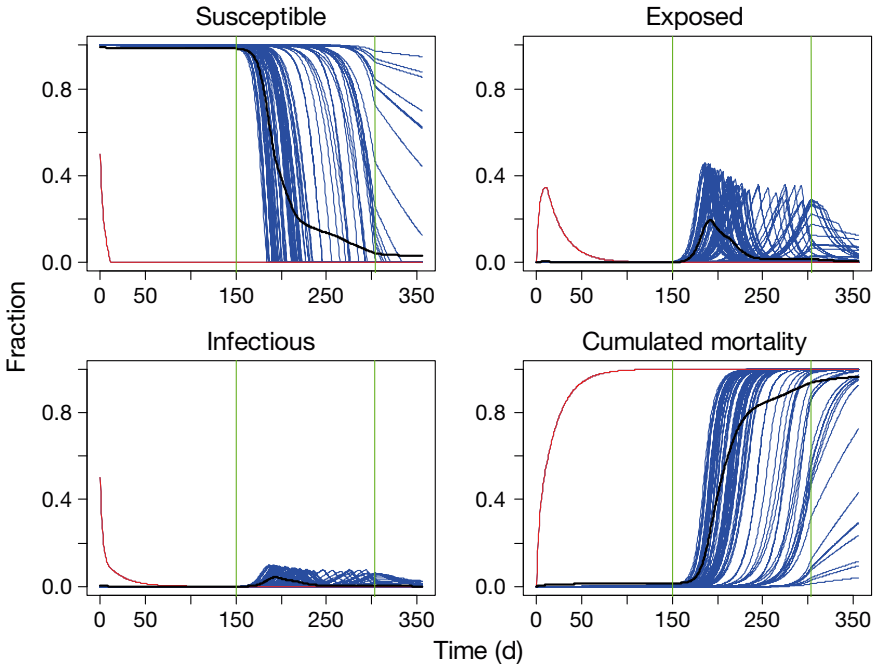

Fig. 4. Reference simulation with 50 % of patch 78 initially infected and cyclic seawater temperature. In each panel, every blue curve shows the trajectory of susceptible, exposed, and infectious states as well as cumulated mortality in each patch, as a fraction of the initial oyster population. Red curves indicate the trajectories for patch 78, black curves indicate the trajectories for the fractions of the total population in each state, and the green lines indicate the timing of high/low/high temperatures in the REF scenario

offset and intensity of mortality in other patches contrasted with the dynamics of the initially infected patch. The decrease in E oysters coincided with the beginning of the summer season in the patches surrounding the patch initially infected. The timing depended on the patch location but the mortality increased dramatically and reached a plateau for almost all patches before the end of the simulated year. The S fraction decreased dramatically from 100 to 20 % during the summer period and decreased slowly afterward. The E and I states peaked in the middle of the summer season. Mortality dramatically increased at the same time, then increased more slowly and reached 100 % at the end of the simulation (1 yr).

These results were summarised by mapping T_{50} in each patch (Fig. 5A). Apart from the initial patch,

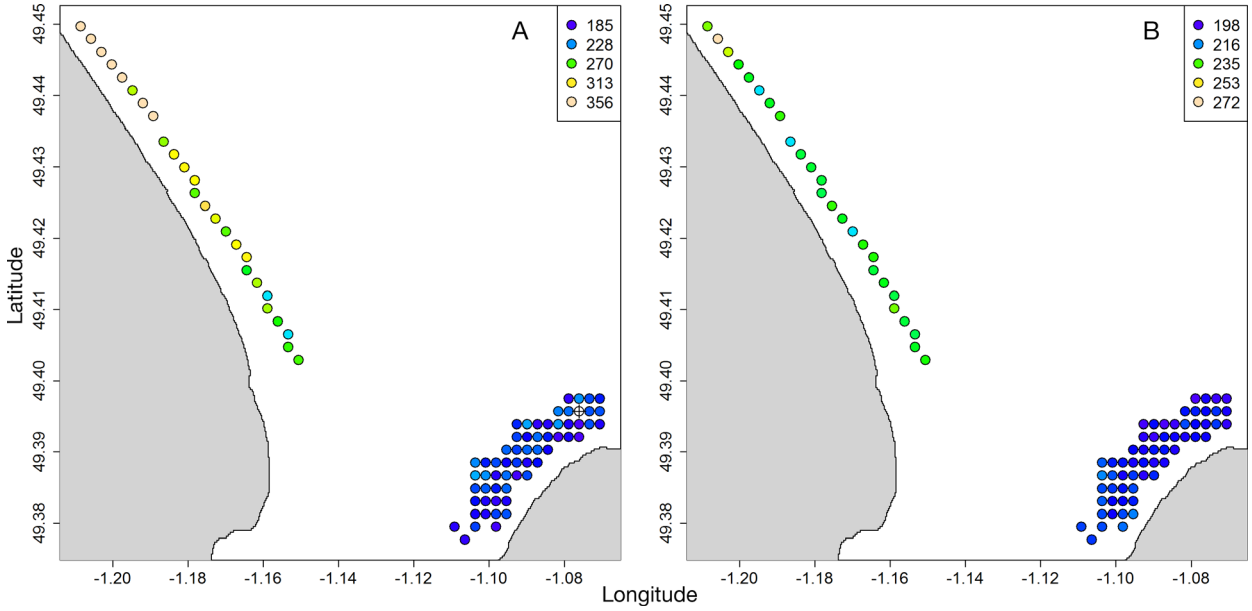

Fig. 5. Maps of the time to obtain 50 % mortality (T_{50}) in days, (A) in each patch, when oysters were initially infected in patch 78 (cross symbol), and (B) computed for simulations with different initial conditions. One simulation was run for each individual patch with the oysters initially infected in this patch. T_{50} of one patch refers to the population summed over all patches for that simulation

where all oysters died within a couple of days, the T_{50} values varied from 187 to 356 d. The map indicated that the oysters located in Grandcamp, i.e. the eastern part of the bay, died more quickly than those located in the western part (Utah Beach).

Similar simulations were carried out with different initial conditions (one initially infected patch at a time). T_{50} varied from 199 to 272 d, depending on the location, and the map showed that it took more time to obtain 50% mortality for initially infected western patches (Fig. 5B).

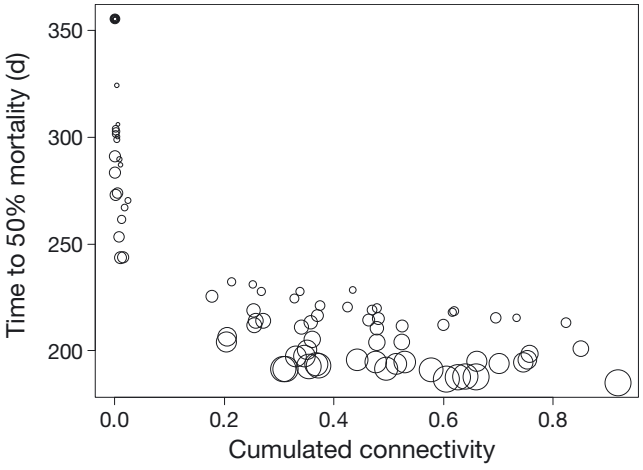

Fig. 6. Plot between the time to obtain 50% mortality in each patch and connectivity between each patch and the patch initially infected in the REF simulation. The size of the circle is proportional to the oyster density in the destination patch

3.2. Marine connectivity effect

The probability of leaving one patch and reaching another patch in 1, 2, or a number of time steps due to hydrodynamics varied over time, but spatial differences were greater than temporal variability (Appendix, Fig. A1). We used the reference simulation where infected oysters were located in patch 78 to assess how connectivity between this patch and others linked to T_{50} in each patch. Therefore, we averaged the connectivity between patch 78 and every other destination patch, and plotted T_{50} versus connectivity (Fig. 6). The lowest T_{50} was obtained for connectivity higher than 0.2. For these connectivity values, T_{50} was between 190 and 240 d, as opposed to T_{50} between 250 and 350 d when connectivity was lower than 0.2. In addition, for destination patches that had a similar connectivity, those with a higher oyster density showed lower T_{50}.

3.3. Temperature effect

The epidemiological states were summed over all patches to yield one trajectory for each oyster population state and each seawater temperature scenario (Fig. 7). Therefore, the initial population state in the patch was defined by S = 50%, I = 50%, E = D = 0%. The LOW scenario resulted in a very low decrease in S and, eventually, a small increase in mortality, which remained very low compared to other scenarios. Under a HIGH scenario, the mortality increased

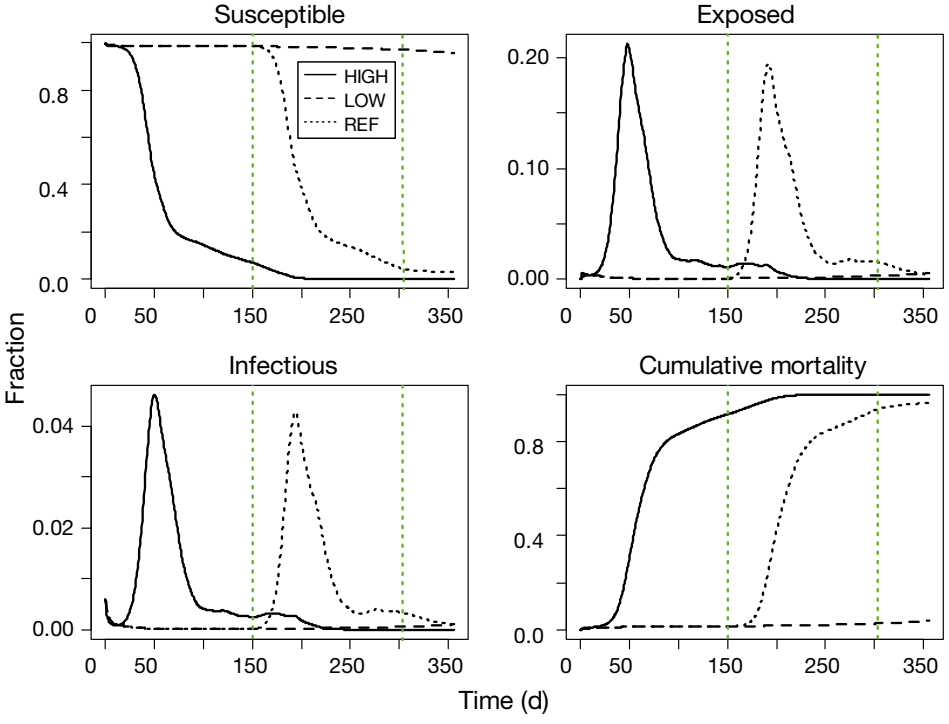

Fig. 7. Dynamics of the epidemiological states susceptible, exposed, infected, and dead (cumulative mortality) calculated for the whole oyster population with 3 temperature scenarios (REF, LOW, HIGH) and the same initial infection in patch 78. The green lines show the timing of high/low/high temperatures in the REF scenario

dramatically after approximately 30 d and reached 100% at around t = 250 d (i.e. mid-August), and all the trajectories displayed a very important shift compared to the REF scenario.

Running simulations with different initial conditions showed that T_{50} varied from 50 to 100 d in the HIGH scenarios compared to the range of 200–270 d in the REF scenarios under cycling temperature (Fig. 8). The 2 series of T_{50} values corresponding to HIGH or REF scenarios were strongly correlated, though the initially infected patches located in the western part of the bay and yielding the highest T_{50} deviated from a linear relationship.

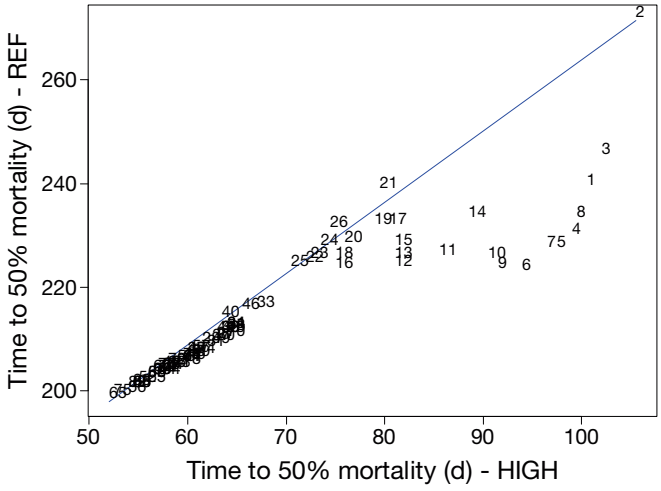

Fig. 8. Comparison between the time to obtain 50% mortality (T_{50}) for different initial conditions and 2 temperature scenarios: REF and HIGH. Each number represents the T_{50} obtained for the 2 scenarios, labelled with the patch number initially infected (1 to 26: eastern part of the bay; 27 to 85: western part of the bay)

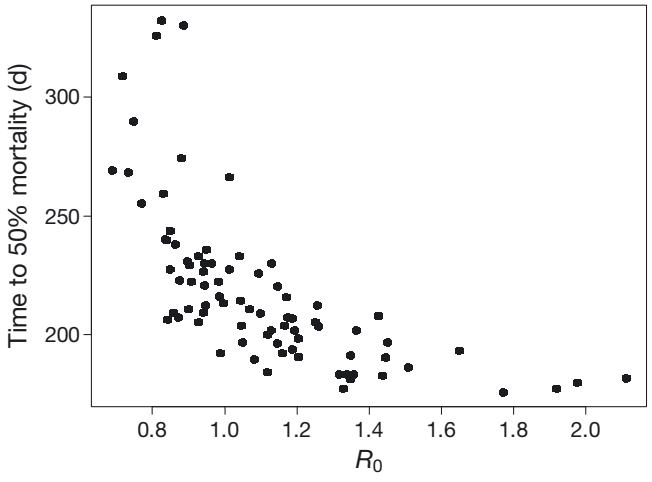

Fig. 9. Simulations with REF conditions run with epidemiological parameters drawn randomly from the observed distributions. Each dot represents a simulation, and the time to obtain 50% mortality was plotted against the contagion parameter R_0

3.4. Uncertainty analysis

The average value of T_{50} was 218 d, with a range of 180 to 330 d. Plotting R_0 versus T_{50} values showed an inverse relationship (Fig. 9). High values of R_0, between 1.5 and 2.2, yielded a T_{50} of less than 180 d, as opposed to a T_{50} of longer than 250 d when R_0 was lower than 0.8.

3.5. The most influential epidemiological parameters

The sensitivity analysis (Fig. 10) showed that K had the greatest influence on T_{50}, and thus, on mortality dynamics, which varied by 140% when the K value at low temperature replaced the value at high temperature. This can be attributed to the difference between K values at high and low temperatures, which were 2 orders of magnitude greater than the difference in other parameters (Fig. 10 and Table 2).

Fig. 11 shows that T_{50} varied by more than 140% when the Q1 value of the shedding rate (e) was used instead of the most probable value at high tempera-

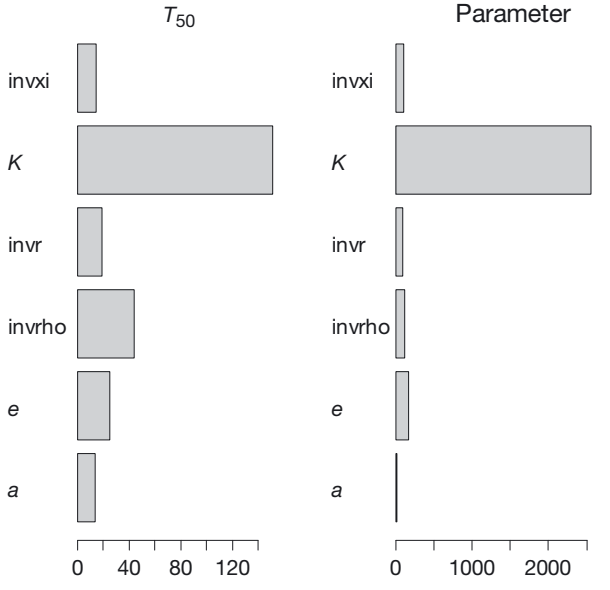

Fig. 10. Sensitivity analysis of the model output to the epidemiological parameters. Left: relative difference (%) of the time to obtain 50% mortality (T_{50}) when parameters at low temperature replaced the value at high temperature. Right: relative difference (%) between low and high temperature values. Parameter names: invrho = 1/ρ ; invxi = 1/ξ ; invr = 1/r (see Table 2)

ture, exceeding the variation of T_{50} for all other epidemiological parameter values.

We combined the results of the sensitivity and uncertainty analyses to assess the relationship between the contagion parameter R_0 and T_{50}. The results showed an inverse relationship (Fig. 12). High values of R_0, between 1.2 and 1.8, would yield a T_{50} between 180 and 200 d, as opposed to a T_{50} between 200 and 250 d when the R_0 was lower than 1.2. Using the Q1 value of *e* at high temperature or the value of *K* at low temperature yielded the highest T_{50} and a R_0 close to 0. Several other parameter changes made R_0 greater than 1.2, but T_{50} remained constant at approximately 200 d.

3.6. Overall model consistency

The conclusions of our simulation experiments are partially supported by the results of a study by Gangnery et al. (2019). Due to the lack of information and data on the source of infection by the pathogens, as the disease is endemic in Baie des Veys, we ran 1 yr simulations with several initial conditions corresponding to the introduction of infected oysters in different locations. All our simulations predicted high mortality levels, e.g. 50% mortality between Day 199 (i.e. mid-July) and Day 272 (i.e. end of September), which is consistent with the second mortality period described by Gangnery et al. (2019) in sentinel oysters. In most of our simulations, the total annual mortality exceeded 90%, but large differences were found between the eastern and western areas of the bay. Initiating the infection in Grandcamp, in the eastern part of the bay, yielded the highest total annual mortality, even if areas in the western part of the bay were less affected, e.g. the T_{50} was much longer, and the final mortality lower than 90% in some of the western areas. Thus, our simulations confirmed the role of the Grandcamp farmed area in the spatial and temporal dynamics of infection and mortality, although the predicted level of mortality was larger than that noted per our observations.

Though Gangnery et al. (2019) showed a statistical relationship between the mortality of adult sentinel oysters and connectivity to Grandcamp oyster farms during the second mortality period only, the results of our model showed that connectivity was a key process allowing pathogens to be transported between farmed areas. Thus, pathogens released by oysters in

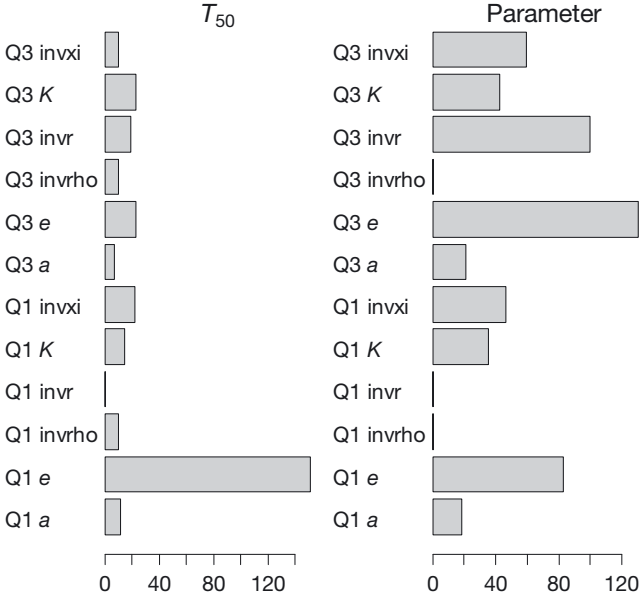

Fig. 11. Variability of the model output depending on the range of each epidemiological parameter. Left: relative difference (%) of the time to obtain 50% mortality (T_{50}) when the most probable value of each epidemiological parameter at high temperature was replaced by the first (Q1) or third (Q3) quartile value of its observed experimental distribution in the REF scenario. Right: relative difference (%) between the most probable and Q1 or Q3 value of each parameter. Parameter name corresponds to the simulation with the corresponding Q value of the parameter's observed experimental distribution. See Fig. 10 for abbreviations

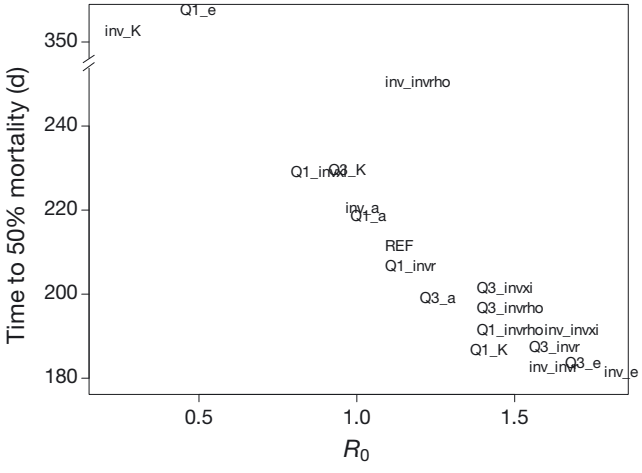

Fig. 12. Sensitivity analysis. Simulations with the REF conditions were run with different sets of epidemiological parameters. Each dot represents a simulation, and the time to obtain 50% mortality (T_{50}) was plotted against the contagion parameter (R_0). The highest T_{50} values correspond to the duration of the simulation (365 d) and are underestimated. Note that the *y*-axis has a break mark and the scale is not continuous. Q_parametername corresponds to the simulation with the corresponding Q value of the parameter's observed experimental distribution; inv_parametername corresponds to a simulation where the value of a parameter at low temperature replaced the value at high temperature. See Fig. 10 for abbreviations

one area have the potential to infect oysters in distant areas, as long as the pathogen concentration exceeds the *K* parameter. We used the same hydrodynamical model as Gangnery et al. (2019) to compute connectivity, but one major difference was that we took into account the temporal variability of connectivity and the lifespan of free-living pathogens. Our simulations showed that the most important pathways connected oyster farms within the Grandcamp area, which resulted in very similar patterns of pathogen transmission and mortality within this area. In addition, connections between Grandcamp and Utah Beach made it possible to transmit pathogens between these 2 regions and trigger mortality with a delay of approximately 2–3 mo (see simulation with initial infection in patch 78). Connections between Utah Beach and Grandcamp areas were weaker, but still allowed the triggering of mortality in Grandcamp and resulted in delayed global annual mortalities.

4. DISCUSSION

4.1. Main results

We first explored the spatiotemporal spread of *Vibrio aestuarianus* and associated oyster mortality and identified the key processes involved in the disease transmission at a bay scale. Results suggest that introducing *V. aestuarianus* in a closed and fully susceptible population of the bay would lead to the complete mortality of farmed oysters in 6 to 12 mo, the duration depending on the location of initial infection. The bacteria spread more rapidly in the eastern part of the bay (Grandcamp) than in the western part (Utah Beach).

In our simulations, the transmission dynamics were triggered by seawater temperature, a widely documented driver of marine infectious diseases (Harvell et al. 2002, Zvuloni et al. 2015), and vibriosis dynamics (Vezzulli et al. 2013). High temperatures may indirectly favour the likelihood of oysters getting infected. On the one hand, oyster susceptibility to *V. aestuarianus* infection may increase with temperature. Indeed, at high temperature, *K* was 25 orders of magnitude lower than that at low temperature, meaning that the probability of acquiring infection was 25-fold greater. On the other hand, the bacterial virulence may be increased, as at high temperature, the *e* was 2 orders of magnitude greater than at low temperature, suggesting a higher host infection burden.

The effect of temperature was captured by R_0. In our model, R_0 was >1 at high temperature (R_0 = 1.22), leading to local transmission of *V. aestuarianus* between oysters, whereas R_0 was <1 (R_0 = 0.41) at low temperature, leading to a stop in infection spread. Gangnery et al. (2019) described a similar local contagion process associated with the field mortality of adult sentinel oysters in summer. Parizadeh et al. (2018) described a temperature limitation of *V. aestuarianus* transmission at around 10°C in a pond.

At the ecosystem scale, the effect of marine connectivity suggested the long-distance dispersal of free-living bacteria. Utah Beach, the western part of the bay, could be theoretically reached by bacteria originating from Grandcamp in the east under a number of modelling scenarios, but the spread time was greatly increased. Such a pattern was expected as the pathogen is waterborne transmitted and short-lived; when the infection starts in the eastern part of the bay, the stepping stone pathogen spread requires more patches to infect, thus, a longer mean time to reach the west. Such long-distance dispersals of marine pathogens have been widely modelled in marine animal diseases (Gustafson et al. 2007, Amundrud & Murray 2009, Kough et al. 2015, Pernet et al. 2018, Samsing et al. 2019). By combining dispersal and epidemiological equations, we went a step forward and showed that dispersal is sufficient to trigger oyster infection and mortality in places distant from the location of initial infection.

In marine ecosystems, infectious disease dynamics are regulated by host population size (Krkosek 2010). A high number of infected hosts can shed a greater number of pathogens, which, in turn, have greater chances of encountering a new host if there are greater numbers of hosts in the immediate environment. A similar role of farm biomass was shown on disease transmission time through hydrodynamic pathways in salmon (Salama & Murray 2013). However, a high host density could also lower the disease transmission rate. Theoretical modelling studies have suggested that the filter-feeding bivalve population may also be sufficiently dense (i.e. over the carrying capacity) to compete for pathogens, reducing the concentration of free-living pathogens below the infective dose, thus limiting epizootic development (Bidegain et al. 2016a,b, Burge et al. 2016, Ben-Horin et al. 2018). Our model only considered the role of infected oysters in the local contagion, and we found that oyster density had a significant and positive effect on the spreading of disease. Accounting for the effect of filtration on pathogen concentration would thus reduce the risk of mortality and could be tested with an equation for the removal of pathogens through filtration by oysters.

4.2. Modelling strategy

Our modelling approach is innovative in assembling different pieces of the puzzle, which were already developed. We scaled up the modelling of the transmission of *V. aestuarianus* in oysters from a local to large scale. We coupled a mathematical transmission model informed by experimental infection data, a spatially dependent model of a distributed oyster population, and a hydrodynamic model formulated using marine connectivity that connected oyster populations by pathogen exchanges.

First, we applied an existing local waterborne transmission model (Lupo et al. 2019) to each oyster population, i.e. oysters present in a patch, which was considered to be closed and homogeneous in terms of host susceptibility and environmental conditions. The transmission parameters used in the local scale model were directly estimated using dedicated laboratory experimental data (Lupo et al. 2019, present study). The use of experimental data was also undertaken to parameterise the transmission model of the protozoan *Perkinsus marinus* in the eastern oyster *Crassostrea virginica* (Bidegain et al. 2017). However, although this model accounted for the seasonal change in disease dynamics, the authors did not explicitly include the temperature effect as we did here. They used specific time factors for processes known to have seasonal dynamics (e.g. pathogen proliferation or inactivation, filtration rate, mortality, recruitment of susceptible oysters).

Second, our model was spatially explicit and formulated using a spatial arrangement of host populations and spatiotemporal pathogen population dynamics. Most of the developed marine molluscan disease models were not spatially structured and assumed a single population (Powell et al. 1996, McCallum et al. 2005, Bidegain et al. 2017). A metapopulation framework, which allows for both movement-based and environmental transmission, was previously adapted for modelling the theoretical transmission of marine diseases (Bidegain & Ben-Horin 2018) and the white plague transmission in corals (Sokolow et al. 2009). However, these models were not spatially explicit. Our modelling strategy lies between these 2 approaches, by connecting oyster populations based on pathogen exchanges but omitting oyster migrations between patches (e.g. anthropogenic movements for farming).

Third, to connect oyster populations by pathogen exchanges, we incorporated the aspect of marine connectivity in our model. We explicitly included free-living bacteria as the transmissible element, using a hydrodynamic connectivity matrix to define the probability of bacteria shed from each patch reaching other patches. This was derived from the Eulerian transport model outputs, run under realistic forcing conditions, from which the survival rate of *V. aestuarianus* in the seawater outside the host (values derived from experimental data) was obtained. Connectivity in marine systems has been modelled using diverse strategies in aquatic animal epidemiology, although the use of particle-tracking models prevails (Murray & Gillibrand 2006, Gustafson et al. 2007, Amundrud & Murray 2009, Kough et al. 2015, Stene et al. 2014) for the use of Euclidean (Brandt & McManus 2009, Zvuloni et al. 2009) or seaway distance (Aldrin et al. 2011).

We assumed infected oysters to be the only explicit reservoir of pathogens, which differs from the methods of Bidegain et al. (2017), who assumed a remote reservoir of pathogens in their transmission model of *P. marinus* in eastern oysters. Contrary to *P. marinus*, for which a plethora of ecological knowledge is available, only a small amount of field data is available regarding the viability of *V. aestuarianus*, and conflicting results have been reported (Azandégbé et al. 2010, Romero et al. 2014, Vezzulli et al. 2015, Parizadeh et al. 2018). This uncertainty surrounding the ecology and host spectrum of *V. aestuarianus* shaped our modelling strategy, resulting in a parsimonious approach.

4.3. Future directions

Our model is based on generic connectivity, local contagion, and disease dynamics, and could be applied to other aquaculture regions, mollusc species, or pathogens. The implementation of such a model to assess a number of management scenarios would contribute to the development of tools, such as the Spatial Information System for Aquaculture, which aims at gathering spatial environmental constraints and regulations in the frame of marine spatial planning (Gangnery et al. in press). Assuming that *V. aestuarianus* is endemic in French oyster populations, scenarios of oyster density, location of oyster farms, temperature range, and connectivity between farms would yield maps of epidemiological risks and assist with defining aquaculture zoning.

Transfer and shuffling actions between growing sites that farmers operate to maintain oyster growth and farm productivity likely increase the risk of pathogen spread. Taking such information into account would make our model more realistic with respect to sanitary risks resulting from the combination of the contagion process and farmer activities. However,

this would require the modification of our model design and the consideration of population units as commercial entities rather than geographical patches. An interesting development would be to move to an agent-based model, such as those developed by Alaliyat et al. (2019).

The sensitivity of oysters to pathogens depends on a number of factors not taken into account in our model. The response of oysters to *V. aestuarianus* infection depends on genetics, age, size, physiological status (Azéma et al. 2016, 2017), and oyster density. Since management plans drive the spatial and temporal arrangement of age classes (maritime register), our model could be improved by integrating a more realistic distribution and structure of an oyster population, which would allow testing scenarios based on spatial arrangements of oyster density. The physiological state of oysters changes over time due to growth and reproduction, and only juvenile and adult oysters are susceptible to *V. aestuarianus* infection (Azéma et al. 2017). An oyster growth model has been implemented in Baie des Veys and was able to reproduce the spatial variability of oyster growth (Grangeré et al. 2010). A general framework, as described by Civitello et al. (2018), could allow the accounting for processes related to host ecophysiology, health, and defence mechanisms.

5. CONCLUSIONS

We demonstrated the relationship between local contagion (measured by the reproduction number) and the speed of mortality spread (assessed as the time until 50% mortality over the whole area). This relationship reflects the upscaling from individuals to the oyster population at the ecosystem scale due to hydrodynamic connectivity. Therefore, our findings show that the risk of mortality is very high throughout the farmed area and would likely extend to a wider domain, posing a risk for aquaculture development in the region.

Additionally, temperature triggers the offset of epidemiology dynamics of *Vibrio aestuarianus* infection. Winter temperatures restrain the intensity of oyster mortality, but a better parameterisation of the relationship between temperature and key epidemiological parameters is necessary to assess the changes in mortality dynamics. Such a development would be particularly interesting in the context of ocean warming, while the phenology of biological and epidemiological processes is expected to change.

Acknowledgements. This work received financial support from the National Research Agency (ANR) within the framework of the GIGASSAT (ANR-12-AGRO-0001) and ENVICOPAS (ANR-15-CE35-0004) projects. Funds for open-access publication fees were received from IFREMER. The postdoctoral research contract of B.L.D. was co-funded by IFREMER and ANR (GIGASSAT project). The oysters used in this work to estimate the epidemiological parameters of *Vibrio aestuarianus* infection were produced by the IFREMER hatchery in Argenton and maintained under controlled conditions at the IFREMER hatchery in La Tremblade and at the IFREMER nursery in Bouin. We are very grateful to the hatchery and nursery teams for their assistance with oyster production. We wish to acknowledge Bruno Petton (IFREMER, Lemar) for his assistance with oyster production.

LITERATURE CITED

Agreste (2015) Recensement de la conchyliculture 2012. In: Agreste Chiffres et Données Agriculture, Book 226 - janvier 2015. Ministère de l'Agriculture, de l'Agroalimentaire et de la Forêt, Montreuil-sous-bois

Alaliyat S, Yndestad H, Davidsen PI (2019) An agent-based approach for predicting patterns of pathogen transmission between aquaculture sites in the Norwegian fjords. Aquaculture 505:98–111

Aldrin M, Lyngstad TM, Kristoffersen AB, Storvik B, Borgan O, Jansen PA (2011) Modelling the spread of infectious salmon anaemia among salmon farms based on seaway distances between farms and genetic relationships between infectious salmon anaemia virus isolates. J R Soc Interface 8:1346–1356

Amundrud TL, Murray AG (2009) Modelling sea lice dispersion under varying environmental forcing in a Scottish sea loch. J Fish Dis 32:27–44

Anderson RM, May RM (1991) Infectious diseases of humans: dynamics and control. Oxford University Press, Oxford

Azandégbé A, Gamier M, Andrieux-Loyer F, Kerouel R, Philippon X, Nicolas JL (2010) Occurrence and seasonality of *Vibrio aestuarianus* in sediment and *Crassostrea gigas* haemolymph at two oyster farms in France. Dis Aquat Org 91:213–221

Azéma P, Travers MA, De Lorgeril J, Tourbiez D, Degremont L (2015) Can selection for resistance to OsHV-1 infection modify susceptibility to *Vibrio aestuarianus* infection in *Crassostrea gigas*? First insights from experimental challenges using primary and successive exposures. Vet Res 46:139

Azéma P, Travers MA, Benabdelmouna A, Degremont L (2016) Single or dual experimental infections with *Vibrio aestuarianus* and OsHV-1 in diploid and triploid *Crassostrea gigas* at the spat, juvenile and adult stages. J Invertebr Pathol 139:92–101

Azéma P, Lamy JB, Boudry P, Renault T, Travers MA, Degrémont L (2017) Genetic parameters of resistance to *Vibrio aestuarianus*, and OsHV-1 infections in the Pacific oyster, *Crassostrea gigas*, at three different life stages. Genet Sel Evol 49:23

Ben-Horin T, Burge CA, Bushek D, Groner ML and others (2018) Intensive oyster aquaculture can reduce disease impacts on sympatric wild oysters. Aquacult Environ Interact 10:557–567

Ben-Horin T, Bidegain G, de Leo G, Groner ML, Hofmann EE, McCallum H, Powell E (2020) Modeling marine dis-

ease. In: Behringer DC, Silliman BR, Lafferty KD (eds) Marine disease ecology. Oxford University Press, Oxford, p 233–256

Bidegain G, Ben-Horin T (2018) Discrete stochastic marine metapopulation disease model. PeerJ Preprints

Bidegain G, Powell EN, Klinck JM, Ben-Horin T, Hofmann EE (2016a) Marine infectious disease dynamics and outbreak thresholds: contact transmission, pandemic infection, and the potential role of filter feeders. Ecosphere 7: e01286

Bidegain G, Powell EN, Klinck JM, Ben-Horin T, Hofmann EE (2016b) Microparasitic disease dynamics in benthic suspension feeders: infective dose, non-focal hosts, and particle diffusion. Ecol Modell 328:44–61

Bidegain G, Powell EN, Klinck JM, Hofmann EE and others (2017) Modeling the transmission of *Perkinsus marinus* in the eastern oyster *Crassostrea virginica*. Fish Res 186: 82–93

Bougrier S, Geairon P, Deslouspaoli JM, Bacher C, Jonquieres G (1995) Allometric relationships and effects of temperature on clearance and oxygen-consumption rates of *Crassostrea gigas* (Thunberg). Aquaculture 134:143–154

Brandt ME, McManus JW (2009) Dynamics and impact of the coral disease white plague: insights from a simulation model. Dis Aquat Org 87:117–133

Buestel D, Ropert M, Prou J, Goulletquer P (2009) History, status, and future of oyster culture in France. J Shellfish Res 28:813–820

Burge CA, Closek CJ, Friedman CS, Groner ML, Jenkins CM, Shore-Maggiok A, Welsh JE (2016) The use of filter-feeders to manage disease in a changing world. Integr Comp Biol 56:573–587

Civitello DJ, Fatima H, Johnson LR, Nisbet RM, Rohr JR (2018) Bioenergetic theory predicts infection dynamics of human schistosomes in intermediate host snails across ecological gradients. Ecol Lett 21:692–701

De Decker S, Reynaud Y, Saulnier D (2013) First molecular evidence of crossspecies induction of metalloprotease gene expression in *Vibrio* strains pathogenic for Pacific oyster *Crassostrea gigas* involving a quorum sensing system. Aquaculture 392–395:1–7

Dufour B, Hendrikx P (2009) The REPAMO in France. In: AEEMA and Editions Quae (ed) Epidemiological surveillance in animal health. OIE-FAO, Paris, p 261–270

EFSA Panel on Animal Health and Welfare (2015) Scientific opinion on oyster mortality EFSA J 13:59

FranceAgriMer (2019) Key figures. The fisheries and aquaculture sector in France

Gangnery A, Normand J, Duval C, Cugier P and others (2019) Connectivities with shellfish farms and channel rivers are associated with mortality risk in oysters. Aquacult Environ Interact 11:493–506

Gangnery A, Bacher C, Boyd A, Liu H, You Y, Strand Ø (in press) Web-based public decision support tool for integrated planning and management in aquaculture. Ocean Coast Manage

Garcia C, Lupo C, Travers MA, Arzul I and others (2014) *Vibrio aestuarianus* and Pacific oyster in France: a review of 10 years of surveillance. National Shellfisheries Association 106th Annual Meeting, March 29–April 2, 2014, Jacksonville, FL

Garnier M, Labreuche Y, Nicolas JL (2008) Molecular and phenotypic characterization of *Vibrio aestuarianus* subsp *francensis* subsp nov., a pathogen of the oyster *Crassostrea gigas.* Syst Appl Microbiol 31:358–365

Girard S, Perez Agundez J, Gangnery A, Vornière JP (2010) Impact of cultural practices on the individual and collective economic performances in shellfish farming: the case of oyster farming in Baie Des Veys. Proc 15th International Institute of Fisheries Economics and Trade (IIFET), Corvallis, OR

Goudenège D, Travers MA, Lemire A, Petton B and others (2015) A single regulatory gene is sufficient to alter *Vibrio aestuarianus* pathogenicity in oysters. Environ Microbiol 17:4189–4199

Grangeré K, Lefebvre S, Bacher C, Cugier P, Ménesguen A (2010) Modelling the spatial heterogeneity of ecological processes in an intertidal estuarine bay: dynamic interactions between bivalves and phytoplankton. Mar Ecol Prog Ser 415:141–158

Gustafson LL, Ellis SK, Beattie MJ, Chang BD and others (2007) Hydrographics and the timing of infectious salmon anemia outbreaks among Atlantic salmon (*Salmo salar* L.) farms in the Quoddy region of Maine, USA and New Brunswick, Canada. Prev Vet Med 78:35–56

Harvell CD, Mitchell CE, Ward JR, Altizer S, Dobson AP, Ostfeld RS, Samuel MD (2002) Climate warming and disease risks for terrestrial and marine biota. Science 296: 2158–2162

Kough AS, Paris CB, Behringer DC, Butler MJ (2015) Modelling the spread and connectivity of waterborne marine pathogens: the case of PaV1 in the Caribbean. ICES J Mar Sci 72:i139–i146

Krkosek M (2010) Host density thresholds and disease control for fisheries and aquaculture. Aquacult Environ Interact 1:21–32

Lasa A, di Cesare A, Tassistro G, Borello A and others (2019) Dynamics of the Pacific oyster pathobiota during mortality episodes in Europe assessed by 16S rRNA gene profiling and a new target enrichment next-generation sequencing strategy. Environ Microbiol 21:4548–4562

Lupo C, Travers MA, Tourbiez D, Barthélémy CF, Beaunée G, Ezanno P (2019) Modeling the transmission of *Vibrio aestuarianus* among Pacific oysters using experimental infection data. Front Vet Sci 6:142

McCallum H, Gerber L, Jani A (2005) Does infectious disease influence the efficacy of marine protected areas? A theoretical framework. J Appl Ecol 42:688–698

Murray AG (2008) Existing and potential use of models in the control and prevention of disease emergencies affecting aquatic animals. Rev Sci Tech 27:211–228

Murray AG, Gillibrand PA (2006) Modelling salmon lice dispersal in Loch Torridon, Scotland. Mar Pollut Bull 53: 128–135

Parizadeh L, Tourbiez D, Garcia C, Haffner P, Degremont L, Le Roux F, Travers MA (2018) Ecologically realistic model of infection for exploring the host damage caused by *Vibrio aestuarianus.* Environ Microbiol 20:4343–4355

Patanasatienkul T, Sanchez J, Davidson J, Revie CW (2019) The application of a mathematical model to evaluate the effectiveness of control strategies against *Ciona intestinalis* in mussel production. Front Vet Sci 6:271

Pernet F, Fuhrmann M, Petton B, Mazurie J and others (2018) Determination of risk factors for herpesvirus outbreak in oysters using a broad-scale spatial epidemiology framework. Sci Rep 8:10869

Powell EN, Hofmann EE (2015) Models of marine molluscan diseases: trends and challenges. J Invertebr Pathol 131: 212–225

Powell EN, Klinck JM, Hofmann EE (1996) Modelling dis-

eased oyster populations. 2. Triggering mechanisms for *Perkinsus marinus* epizootics. J Shellfish Res 15:141–165

Préfecture de la Manche (2013) Arrêté modificatif CM 13-032 de l'arrêté préfectoral n°04-04-621 modifié en dernier lieu le 15 février 2013 portant schéma des structures des exploitations de cultures marines du département de la Manche, Préfecture de la Manche, Saint-Lô

Préfecture du Calvados (2007) Arrêté N°80/2007 portant schéma des structures des exploitations de cultures marines du département du Calvados, Préfecture du Calvados, Caen

REPHY (2017) REPHY dataset — French Observation and Monitoring program for Phytoplankton and Hydrology in coastal waters. 1987–2016 Metropolitan data. SEANOE, https://doi.org/10.17882/47248

Romero A, Costa MD, Forn-Cuni G, Balseiro P and others (2014) Occurrence, seasonality and infectivity of *Vibrio* strains in natural populations of mussels *Mytilus galloprovincialis*. Dis Aquat Org 108:149–163

Salama NK, Murray AG (2013) A comparison of modelling approaches to assess the transmission of pathogens between Scottish fish farms: the role of hydrodynamics and site biomass. Prev Vet Med 108:285–293

Salama NKG, Rabe B (2013) Developing models for investigating the environmental transmission of disease-causing agents within open-cage salmon aquaculture. Aquacult Environ Interact 4:91–115

Samsing F, Johnsen I, Treml EA, Dempster T (2019) Identifying 'firebreaks' to fragment dispersal networks of a marine parasite. Int J Parasitol 49:277–286

Segarra A, Pepin JF, Arzul I, Morga B, Faury N, Renault T (2010) Detection and description of a particular Ostreid herpesvirus 1 genotype associated with massive mortality outbreaks of Pacific oysters, *Crassostrea gigas*, in France in 2008. Virus Res 153:92–99

Shigematsu M, Meno Y, Misumi H, Amako K (1995) The measurement of swimming velocity of *Vibrio cholerae* and *Pseudomonas aeruginosa* using the video tracking methods. Microbiol Immunol 39:741–744

Sokolow SH, Foley P, Foley JE, Hastings A, Richardson LL (2009) Disease dynamics in marine metapopulations: modelling infectious diseases on coral reefs. J Appl Ecol 46:621–631

Stene A, Viljugrein H, Yndestad H, Tavornpanich S, Skjerve E (2014) Transmission dynamics of pancreas disease (PD) in a Norwegian fjord: aspects of water transport, contact networks and infection pressure among salmon farms. J Fish Dis 37:123–134

Thompson RN, Brooks-Pollock E (2019) Detection, forecasting and control of infectious disease epidemics: modelling outbreaks in humans, animals and plants. Philos Trans R Soc Lond B Biol Sci 374:20190038

Travers MA, Tourbiez D, Parizadeh L, Haffner P and others (2017) Several strains, one disease: experimental investigation of *Vibrio aestuarianus* infection parameters in the Pacific oyster, *Crassostrea gigas*. Vet Res 48:32

Vezzulli L, Colwell RR, Pruzzo C (2013) Ocean warming and spread of pathogenic vibrios in the aquatic environment. Microb Ecol 65:817–825

Vezzulli L, Pezzati E, Stauder M, Stagnaro L, Venier P, Pruzzo C (2015) Aquatic ecology of the oyster pathogens *Vibrio splendidus* and *Vibrio aestuarianus.* Environ Microbiol 17:1065–1080

Walters C, Meslé M, Hall I (2018) Modelling the global spread of diseases: a review of current practice and capability. Epidemics 25:1–8

Zvuloni A, Artzy-Randrup Y, Stone L, Kramarsky-Winter E, Barkan R, Loya Y (2009) Spatio-temporal transmission patterns of black-band disease in a coral community. PLOS ONE 4:e4993

Appendix

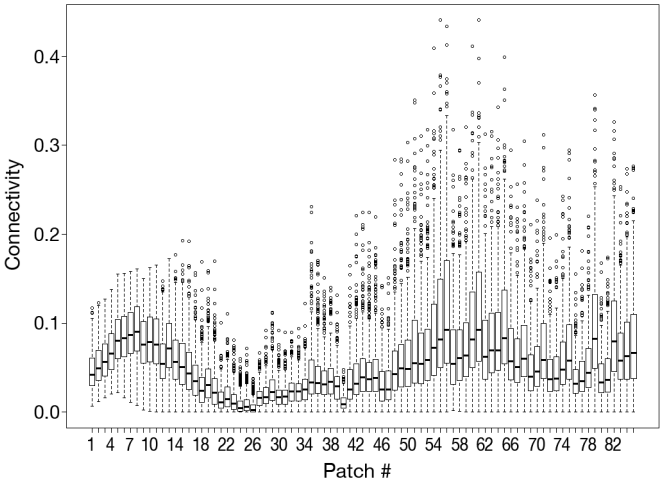

Fig. A1. Distribution of total connectivity between one patch and all other patches of the domain. The probabilities of leaving one patch and reaching another patch in one or several days have been summed up at each time step. Results show the high variability of connectivity due to the changes of the hydrodynamic conditions. They also highlight that patches 21 to 26 have the lowest connectivity, with average values close to 0. The connectivity matrix was of dimensions $L \times M \times N \times P$, where L is the number of dates, N is the number of emission patches, and P is the number of reception patches ($N=P$ in these simulations). The connectivity matrix used was as follows: Connectivity[30,10,20,50] represents: day no. 30; time step no. 10 (i.e. 10×12 h = 120 h after release; emission from patch 20; and reception at patch 50. For instance, Connectivity [30,10,20,50] = 0.001 indicates that if one pathogen was released at the beginning of run 30 from patch 20, the probability that the pathogen will reach patch 50 after 120 h is 0.001

Editorial responsibility: Kate S. Hutson, Nelson, New Zealand

Submitted: March 31, 2020; Accepted: September 11, 2020
Proofs received from author(s): November 10, 2020